ACS OMEGA

Open Access

http://pubs.acs.org/journal/acsodf

Article

Intrinsic Room-Temperature Ferromagnetism in New Halide Perovskite $AgCrX_3$ (X: F, Cl, Br, I) Using Ab Initio and Monte Carlo Simulations

Muhammad Ahmad, Akhtar Rasool, Muhammad Abdul,* Altaf Ur Rahman,* Misbah Ullah Khan, Mohammad N. Murshed, Mohamed E. El Sayed, Muhammad Ashfaq Ahmad, and Bao Jingfu*

Cite This: *ACS Omega* 2024, 9, 18148−18159

Read Online

ACCESS | Metrics & More | Article Recommendations | Supporting Information

ABSTRACT: Herein, we present a detailed comparative study of the structural, elastic, electronic, and magnetic properties of a series of new halide perovskite $AgCrX_3$ (X: F, Cl, Br, I) crystal structures using density functional theory, mean-field theory (MFT), and quantum Monte Carlo (MC) simulations. As demonstrated by the negative formation energy and Born−Huang stability criteria, the suggested perovskite compounds show potential stability in the cubic crystal structure. The materials are ductile because the Pugh's ratio is greater than 1.75, and the Cauchy pressure ($C_{12}-C_{44}$) is positive. The ground state magnetic moments of the compound were calculated as 3.70, 3.91, 3.92, and 3.91 μ_B for $AgCrF_3$, $AgCrCl_3$, $AgCrBr_3$, and $AgCrI_3$, respectively. The GGA + SOC computed spin-polarized electronic structures reveal ferromagnetism and confirm the metallic character in all of these compounds under consideration. These characteristics are robust under a ±3% strained lattice constant. Using relativistic pseudopotentials, the total energy is calculated, which yields that the single ion anisotropy is 0.004 meV and the *z*-axis is the hard-axis in the series of $AgCrX_3$ (X: F, Cl, Br, and I) compounds. Further, to explore room-temperature intrinsic ferromagnetism, we considered ferromagnetic and antiferromagnetic interactions of the magnetic ions in the compounds by considering a supercell with 2 × 2 × 2 dimensions. The transition temperature is estimated by two models, namely, MFT and MC simulations. The calculated Curie temperatures using MC simulations are 518.35, 624.30, 517.94, and 497.28 K, with ±5% error for $AgCrF_3$, $AgCrCl_3$, $AgCrBr_3$, and $AgCrI_3$ compounds, respectively. Our results suggest that halide perovskite $AgCrX_3$ compounds are promising materials for spintronic nanodevices at room temperature and provide new recommendations. For the first time, we report results for novel halide perovskite compounds based on Ag and Cr atoms.

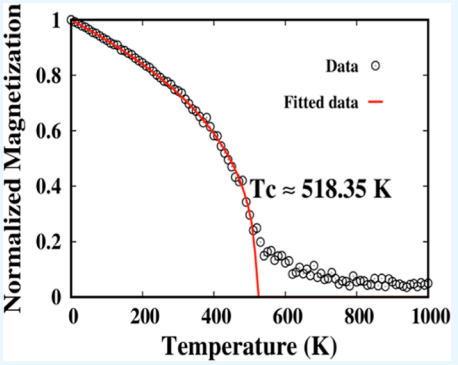

1. INTRODUCTION

The development of modern technologies demands that the processing and storage of information be done with extreme efficiency. Future research in this area is going to concentrate on spintronics (also known as "spin-based electronics"), which differentiates itself from conventional electronics by considering electron spin to be a new kind of "degree of freedom." High spin polarization magnetic materials are often the best choice in spintronic devices.[1,2] To create novel spintronic devices, magnetic semiconductors or spin-injecting half-metals have inspired the study of magnetism. Modern spintronic applications,[3] which include GMR,[4] MRAM, spin valves, and magnetic sensors, effectively utilize half-metallic (HM) ferromagnetic materials as a result of recent improvements in spintronic innovation.[5,6] De Groot et al., discovery of half-metallic ferromagnetism in (Pt/Ni)MnSb Heusler alloys for the first time in 1983 opened up an entirely novel area for research.[7] Since then, the phenomenon of HMF in spinel chalcogenides, along with single and DPs, has been the topic of extensive theoretical and experimental research.[8,9] Binary and ternary oxides, such as MgO,[10] CaO,[11] ZnO,[12] $SrTiO_2$,[13] BeO,[14] SiO_2,[15] and other compounds,[16,17] have been found to demonstrate magnetism.

For this purpose, cubic perovskite-related materials with the general formula ABX_3 have been considered, where A ions can be rare earth, alkaline earth, alkali, or other large ions involving Pb^{2+} and Bi^{3+}, and B ions could be transitional metal ions of the 3d, 4d, or 5d, which fit into the octahedral sites. X represents oxygen or halogens (F, Cl, Br, I), which are anions.[18,19] Perovskite materials offer fascinating features due to their variable structure and composition, such as tremendous magnetoresistance, high magneto capacitance, and multiferroicity. As a result, they have inspired a lot of applied and fundamental fields like chemistry,[20] physics,[21]

Received: December 19, 2023
Revised: March 14, 2024
Accepted: March 25, 2024
Published: April 9, 2024

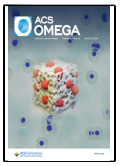

advanced materials,[22] as well as other fields. The lead-containing perovskite compounds are poisonous and dangerous despite their potential in photoluminescence applications. The structural, electrical, optical, and mechanical characteristics of a material, among others, are often studied in detail to understand the challenges associated with its use in certain applications. Scientific communities may take notice of lead-free halide perovskites as a viable alternative.[23,24] To predict a material's potential applications, its physical features are often investigated using experimental and theoretical approaches.[25,26] Perovskite materials, which are made up of insulators, semiconductors, and even superconductors,[27,28] show some of the many potential uses for photocatalytic, dielectric, ferroelectric, pyroelectric, piezoelectric, magnetic, superconductivity, and ionic conductivity.[29−31]

In recent times, researchers have been in pursuit of developing innovative spintronic devices. Lin et al. predicted that the $NbBaMn_2O_6$ compound could have a maximum magnetic moment of 10 μ_B/fu with a half-metallic (band gap of 1.43 eV in spin down channel).[32] Similarly, Dar et al. explored a series of Cs_2KXCl_6: (X = Ti and V) compounds and found that Ti-based compounds had a magnetic moment of 1 μ_B per cell, while compounds based on vanadium had 2 μ_B per cell.[33] So materials applicable for spintronic devices should have high degree of spin polarization, i.e, a large magnetic moment. We hope for a high magnetic moment in Ag and Cr based halide perovskite compounds. It was discovered that most of the cubic perovskites had an isotropic and mechanically stable nature. However, more research is required at all levels to explore their potential in existing crystals or to create new crystals that can satisfy all of the criteria for practical spintronic applications. Though there have been theoretical and experimental attempts to forecast a potential candidate for nanoelectronic and spintronic devices, it is challenging to realize 3D materials with outstanding electronic and magnetic properties at room temperature.

This research project will explore the properties of the newly predicted halide $AgCrX_3$ (X: F, Cl, Br, and I) compounds. Our investigation will cover the compound's structural, phonon band structure, mechanical, electronic, and magnetic properties. We will also examine how the application of strain affects its magnetic characteristics. To determine the system's most stable state and the presence of room temperature ferromagnetism, we will analyze the ferromagnetic (FM) and antiferromagnetic (AFM) coupling between magnetic atoms in $AgCrX_3$ (X: F, Cl, Br, I) compounds. Additionally, we will forecast the transition temperature using mean-field theory (MFT) and quantum Monte Carlo simulations while utilizing the exchange interactions constant. This study will allow the investigated compounds to have practical uses for feasible electronic and spintronic device applications.

2. COMPUTATIONAL METHODOLOGY

First-principles simulations were conducted using the Quantum-Espresso code.[34] The plane-wave pseudopotential method was used for density functional theory (DFT) calculations.[35] The exchange and correlation energy was determined using the generalized gradient approximation (GGA + SOC) proposed by Perdew, Burke, and Ernzerhof,[36] along with the hybrid functional developed by Heyd, Scuseria, and Ernzerhof.[37] In the pseudoatomic computation, the number of valence electrons considered were 1 for Ag ($4d^{10} + 5s^1$), 4 for Cr ($3d^4 + 4s^2$), and 1 for each element X, such as F ($2s^2 + 2p^5$), Cl ($3s^2 + 3p^5$), Br ($4s^2 + 4s^5$), and I ($5s^2 + 5s^5$). The electron wave function was computed as a plane-wave basis set, with optimal values of the wave function and charge density cutoff set at 50 and 220 Ry, respectively. To sample from the Brillouin region, the Monkhorst−Pack technique was used.[38] The convergence of the findings was carefully verified for all computations. The Hellmann−Feynman (HF) force on each atom was reduced to less than 10^{-3} Ry/Bohr, and then, the structures were considered relaxed. The formation energy of bulk $AgCrX_3$ was defined as

$$E_f = [E_{tot}^{AgCrX_3} - (aE_{Ag}^{bulk} + bE_{Cr}^{bulk} + cE_X^{bulk})]/(a + b + c) \quad (1)$$

where $E_{tot}^{AgCrX_3}$ represents the total energy of the crystal structure $AgCrX_3$ per unit cell under the steady-state equilibrium conditions. The E_{Ag}^{bulk}, E_{Cr}^{bulk}, and E_X^{bulk} is energy per atom, calculated from the Ag[FCC], Cr[BCC], and X molecular phases, respectively, where a, b, and c are integers that indicate the number of Ag-atoms, Cr-atoms, and X atoms per unit cubic cell, respectively.

3. RESULTS AND DISCUSSION

3.1. Crystal Structure. The halide perovskite material that has been presented in Figure 1a has a cubic crystal structure

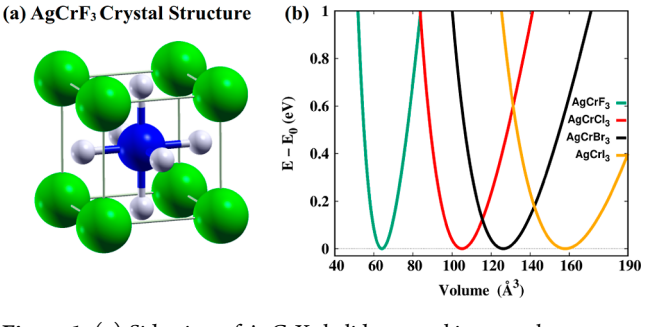

Figure 1. (a) Side-view of $AgCrX_3$ halide perovskite crystal structures, where Ag, Cr, and X (F, Cl, Be, and I) atoms are represented by green, blue, and white spheres, respectively. (b) Green, red, black, and orange lines represent the volume optimization of $AgCrF_3$, $AgCrCl_3$, $AgCrBr_3$, and $AgCrI_3$ compounds, respectively.

and belongs to the space group $Pm\bar{3}m$ (#221). It has five atoms per unit cell of $AgCrX_3$ (X: F, Cl, Br, I) perovskite compounds. Among these, the Ag atom is placed at the corner, the Cr atom is placed at the body-centered, and the X (F, Cl, Br, I) atoms are positioned at the adjacent face-centered sites. To investigate the structural, electronic, and magnetic characteristics of $AgCrX_3$ (X: F, Cl, Br, I) compounds, we first did optimization, i.e., calculated the total energy as a function of unit-cell volume. By lowering a material's crystal energy relative to its unit cell volume, one may utilize first-principles simulations to find the ground-state energy and lattice parameters. The calculated total energies by varying unit cell volume are fitted using Birch−Murnaghan's curve approach.[39,40] Figure 1b depicts the volume optimization curves for all of the investigated compounds. Table 1 listed the optimized lattice constants of $AgCrF_3$, $AgCrCl_3$, $AgCrBr_3$, and $AgCrI_3$ are 4.002 4.718, 5.016, and 5.405 Å, respectively. By comparing the lattice parameters, it is found that they are enhanced when moving from F to I because the atomic sizes (electronegativity) increase (decrease) across the group. To check the thermodynamic stability at equilibrium, the lattice

https://doi.org/10.1021/acsomega.3c10174
ACS Omega 2024, 9, 18148−18159

Table 1. Optimized Lattice Constant (a_o) is in the Unit of Å, Optimal Volume V_o in a Unit of Å^3, Formation Energy (E_f) in a Unit of eV, the Local Magnetic Moment of the Cr Atoms and Total Magnetic Moments of $AgCrX_3$ (X: F, Cl, Br, I) Compounds are in the Unit of μ_B

sample	a_o	V_o	E_f	μ_{tot} (μ_{Cr})
$AgCrF_3$	4.00	64.09	−0.28	3.70 (3.57)
	3.96[41]		−1.15[41]	[5.00,4.00,3.00,1.99][42]
$AgCrCl_3$	4.71	105.02	−0.20	3.91 (3.75)
	5.31[43]	195.60[44]	−1.85[45]	[4.00,5.00][46]
$AgCrBr_3$	5.01	126.20	−0.17	3.92 (3.78)
	5.53[47]	223.72[44]	−1.43[45]	2.00[48]
$AgCrI_3$	5.40	157.90	−0.14	3.91 (3.82)
	5.99[47]	259.596[44]	[−1.16][49]	4.00[50]

constant formation energy is calculated with respect to its constituent atoms and has been tabulated in Table 1. The formation energies are negative for all studied compounds, indicating that all these compounds are thermodynamically stable. We also considered magnetic and nonmagnetic calculations and found that all these compounds have a magnetic ground state. A negative formation energy suggests that these compounds in the experiment may grow spontaneously through an exothermic reaction in which energy is released.

These compounds are being investigated for the first time, and no data are available in the literature. The physical and chemical properties arise due to the valence electron contribution, which participates in bonding. Therefore, compounds with similar family members from the periodic table of elements tend to have similar characteristics. For this reason, we compared our findings with nearly matching perovskite compounds. For example, let us compare $AgCrF_3$ with $AgCoF_3$ and $AgNiF_3$, metallic and semiconducting compounds. They have lattice constants of 3.96 and 3.93 Å with total magnetic moments of 3.04 and 2.00 μ_B in the cubic phase. While if we compare $AgCrF_3$ with a series of perovskite KMF_3 (M; Mn, Fe, Co, Ni) compounds, they have optimized lattice constants of 4.19, 4.06, 4.04, and 4.01 Å for $KMnF_3$, $KFeF_3$, $KCoF_3$, and $KNiF_3$, respectively. Table 1 lists our computed values of magnetic moments compared with those of a series of perovskite KMF_3 compounds. Similarly, the lattice constant of $AgCrCl_3$ can be compared to $CsPbCl_3$, the magnetic moment with the $RbCrCl_3$, $KCrCl_3$, and $KMnCl_3$, which are 4.00, 4.00, and 5.00 μ_B, respectively.[46] By comparing the compound $AgCrBr_3$ with $CsCdBr_3$, which has a lattice constant of 5.53 Å. Similarly, the compounds $XTiBr_3$ (X = Rb, Cs) which having the magnetic moments of 1.99 μ_B and 2.00 μ_B with GGA calculations.[48,50] On comparing the $AgCrI_3$ with $RbCrI_3$ and $CsCrI_3$ having magnetic moments 4.00 μ_B per unit cell.[50]

3.2. Mechanical Properties. Elastic constants are physical quantities that reveal a material's mechanical properties and how it responds to external forces. For the cubic system, there are three independent elastic constants, C_{ij}: C_{11}, C_{12}, and C_{44}. The stiffness matrix of rank two having 36 components is composed of three independent elastic constants in the case of cubic crystal structure. The stiffness matrix components are denoted by the notation C_{ij}, where i and j are indices that represent the direction in which stress or strain is being applied. By examining the energy variation that results from applying a slight strain to the unstrained lattice, one can derive these constants.[51] The constant C_{11} is related to unidirectional compression along the primary crystallographic directions, while C_{12} and C_{44} are connected to shear deformation resistance. In the case of the mentioned material, $AgCrX_3$ (X: F, Cl, Br, I), $AgCrCl_3$ possesses the highest C_{11} compared to other compounds. It suggests that the compound is fairly rigid and resistant to deformation in a direction parallel to a certain crystallographic axis. The material will have a high modulus of elasticity and increased stiffness, as the value of C_{11} is high, suggesting a strong bond between the atoms and ions in the material. While $AgCrBr_3$ gains second position in rigidity and withstand to deformation as the value of C_{11} is less than that of C_{11} of $AgCrCl_3$. While in the remaining two compounds ($AgCrF_3$ and $AgCrI_3$), $AgCrF_3$ shows a higher C_{11}'s value than $AgCrI_3$ does. In the studied material $AgCrCl_3$, the value of constant C_{12} is again larger compared to others, which means that in a particular crystallographic plane, the material $AgCrCl_3$ exhibits strong resistance to shear deformation, so the material holds the ability to resist shearing forces that are applied perpendicular to a certain axis or direction in its crystal structure. This suggests a strong link between the atoms or ions in that plane and that they cannot easily slide or slip. The constants C_{12} of compounds $AgCrI_3$, $AgCrF_3$, and $AgCrBr_3$ gain the second, third, and fourth largest values compared to $AgCrCl_3$, while compound $AgCrF_3$ has the largest value of constant C_{44} than other mentioned compounds ($AgCrCl_3$, $AgCrBr_3$, and $AgCrI_3$). In this article, the three independent elastic constants, C_{11}, C_{12} and C_{44}, are enough to fulfill the Born-Huang criteria of stability. These values for $AgCrX_3$ (X: F, Cl, Br, and I) are given in Table 2.

Table 2. Elastic Constants of $AgCrX_3$ (X: F, Cl, Br, I) Perovskite Compounds in Unit of GPa

elastic constant	$AgCrF_3$	$AgCrCl_3$	$AgCrBr_3$	$AgCrI_3$
C_{11}	48.69	93.15	74.77	47.49
C_{12}	17.54	24.16	16.67	21.20
C_{44}	13.81	11.18	9.32	6.86
C11C44	3.52	8.32	8.01	6.91

The ratio $\left(\frac{C_{11}}{C_{44}}\right)$ of a material's stiffness is in a direction perpendicular to that in which it possesses the highest stiffness. A series of parameters known as Born−Huang stability criteria must be met for a crystal lattice to be mechanically stable. According to the following equations, the Born−Huang criteria for cubic crystal stability can be derived[52,53]

$$C_{11} + 2C_{12} > 0, \quad C_{44} > 0, \quad C_{11} - C_{12} > 0 \tag{2}$$

The standards are based on how elastic the lattice is and how much force it takes to bend it. The compound $AgCrX_3$ (X: F, Cl, Br, and I) has positive lattice elastic constants; this demonstrates that spontaneous compression or shear deformation cannot impact the lattice very easily. So, the lattice possesses more energy overall than the sum of the energies of the individual atoms that make it up. The atoms are kept together by cohesive forces as a result, ensuring that the lattice is energetically stable. Stiffness and compressibility are two fundamental mechanical properties of materials that determine their behavior under stress and deformation. The ability to resist deformation is measured by stiffness,[54] whereas the capacity to change volume in response to applied pressure or stress is measured by compressibility.[55] Poisson's ratio

https://doi.org/10.1021/acsomega.3c10174
ACS Omega 2024, 9, 18148−18159

describes the link between stiffness and compressibility, which is the ratio of the lateral stresses and axial strains that occur when a material is exposed to external loads. When comparing the elastic constants C_{11}, C_{12} and C_{44}, it can be seen that $AgCrX_3$ (X: F, Cl, Br, I) is less compressible in the x direction, as C_{11} is larger than C_{12} and C_{44}. The bulk modulus and the shear modulus establish the material's mechanical characteristics. The bulk modulus is defined as the ratio between the pressure exerted and the proportional shift in volume that occurs as a consequence.[56] The letter "B" is often used to signify the bulk modulus. The bulk modulus may be calculated using the two independent elastic constants C_{11} and C_{12}

$$B = \frac{C_{11} + 2C_{12}}{3} \tag{3}$$

The bulk modulus measures a compound's hardness, and the values listed in Table 3 indicate the hardness of the material

Table 3. Various Moduli of a Series of $AgCrX_3$ (X: F, Cl, Br, I) Compounds

modulus	$AgCrF_3$	$AgCrCl_3$	$AgCrBr_3$	$AgCrI_3$
B	27.92	47.16	36.04	29.96[16.5][57]
	92.68[41]	31.9[57]	21.0[57]	16.5[57]
G_V	14.51	20.50	17.21	9.37
G_R	0.30	0.33	0.34	0.27
G_H	7.40	10.42	8.78[	4.82
	10.01[41]	14.15[43]	6.56[45]	4.197[44]

$AgCrX_3$ (X: F, Cl, Br, and I). It shows that $AgCrCl_3$ has the highest value of bulk modulus, which means that it is the hardest studied material in this study. Meanwhile, $AgCrBr_3$ is the second hardest compound in the examined material, $AgCrX_3$ (X: F, Cl, Br, I). The remaining two compounds, $AgCrI_3$ and $AgCrF_3$, are comparatively less hard than the previous ones. Through a comparative analysis of the bulk modulus values of $AgCrF_3$, $AgCoF_3$, and $AgNiF_3$, it can be deduced that the latter two compounds exhibit higher levels of hardness in comparison to $AgCrF_3$, as shown by their greater bulk modulus values. Comparably, we may make a comparison between the bulk moduli of $AgCrCl_3$, $AgCrBr_3$, and $AgCrI_3$ with those of $CsCdCl_3$, $CsPbCl_3$, $CsPbBr_3$, and $CsPbI_3$, respectively. This comparison reveals that the compounds mentioned above exhibit a lower hardness than $AgCrCl_3$, $AgCrBr_3$, and $AgCrI_3$, as shown in Table 3.

The shear modulus is the modulus of rigidity. The Hill approximation can be employed for estimating a material's shear modulus. The resistance of a material to shear stress-induced deformation is indicated by its shear modulus. Shear pressures more readily distort materials with low shear moduli, while high shear modulus materials are stiffer and more resistant to shearing forces. By comparing (in Table 3) $AgCrF_3$ with $AgMF_3$ (M = Co, Ni), results show that the compounds $AgMF_3$ are stiffer and quite resistant to shear forces. In addition, comparing the shear modulus of $AgCrCl_3$ with that of $CsCaCl_3$ and $CsCdCl_3$ indicates that these two compounds are more resistant to shear strength. Further, the compound $AgCrBr_3$ is more resistant than $KGeBr_3$ but less resistant than $RbGeBr_3$ and $CsGeBr_3$, as they have higher values of shear moduli. Furthermore, Hill approximations can be used to find the approximate values for the shear modulus of a given material as follows

$$G_H = \frac{G_R + G_V}{2} \tag{4}$$

where G_R represents the Reuss approximation (modulus), whereas G_V is the Voigt approximation (modulus), $AgCrI_3$ has higher values of G_H, making it a more resistant material than $LiPbI_3$, as shown in Table 3. Equations 5 and 6 represent the mathematical expressions of Reuss and Voigt approximations.[58]

$$G_V = \frac{C_{11} - C_{12} + 3C_{44}}{5} \tag{5}$$

The Voigt approximation is a technique used for determining the shear modulus upper bound and the effective elastic properties of composite materials. The composite material is supposed to be transversely isotropic and to comprise two components with equal volume fractions in this approximation. A technique for evaluating the lower bound of a composite material's effective elastic aspects is the Reuss approximation. It is probably accurate to say that the composite material behaves as if it were a homogeneous component with isotropic properties. The Reuss approximation is mathematically represented as

$$G_R = \frac{(C_{11} - C_{12})5C_{44}}{4C_{44}(3C_{11} - C_{12})} \tag{6}$$

It is a variation in a material's physical characteristics when measured along different axes.[59] Materials that are isotropic have an A value of 1, whereas materials that are anisotropic have an A value that is higher or lower than 1. This may happen as a result of variations in the crystal structure, grain orientation, fiber alignment, or other elements that have an impact on the material's physical behavior. The mathematical formula for anisotropy is[60]

$$A = \frac{2C_{44}}{C_{11} - C_{12}} \tag{7}$$

The values of anisotropy of $AgCrF_3$, $AgCrCl_3$, $AgCrBr_3$, and $AgCrI_3$ are 0.88, 0.33, 0.32, and 0.52, respectively, showing that they are all anisotropic compounds. In Table 3, a comparison of the anisotropic values of these materials with others is mentioned, which indicates that $AgCrF_3$ has higher anisotropic values than $AgCoF_3$ and $AgCrF_3$, which implies that the $AgCrF_3$'s behavior (stiffness or strength) changes considerably when measured in different directions. This could mean that $AgCrF_3$ might be stronger or stiffer along one axis compared to another. This behavior can also be seen for $AgCrI_3$ while comparing it with $LiPbI_3$. On the other hand, $AgCrCl_3$ has less anisotropic values than $CsCaCl_3$ (GGA approximations), but higher than $CsCdCl_3$ which has negative anisotropic values. The anisotropic behavior of $AgCrBr_3$ is quite interesting as its anisotropy values are higher than $KGeBr_3$ but less than $RbGeBr_3$ and $CsGeBr_3$, making it stiffer or stronger than $KGeBr_3$, but less than $RbGeBr_3$ and $CsGeBr_3$. Two mechanical characteristics of materials that go against one another are ductility and brittleness. The degree to which a material resists plastic deformation under tensile stress before collapsing is called ductility.[61] When a material is said to be brittle, it has a small tendency to deform before breaking under stress but cracks when put under stress.[62] The Young Modulus, Pugh's ratio, and Poisson's ratio are the parameters for evaluating brittleness. These are discussed in more detail in the following

https://doi.org/10.1021/acsomega.3c10174
ACS Omega 2024, 9, 18148−18159

paragraphs. The resistance (stiffness) of an elastic solid to a change in length may be measured using Young's Modulus, also known as the stress-to-strain ratio.[63] Young's Modulus can be expressed mathematically as

$$E = \frac{9GB}{3G + B} \tag{8}$$

In the present study (see Table 4), Young's modulus of $AgCrF_3$ (37.12) is higher than that of $AgNiF_3$ (28.99) but less

Table 4. Mechanical Parameters of $AgCrX_3$ (X: F, Cl, Br, I) Halide Perovskite Compounds

modulus	$AgCrF_3$	$AgCrCl_3$	$AgCrBr_3$	$AgCrI_3$
A	0.88	0.33	0.32	0.52
	0.54[41]	0.43[70]	0.41[45]	0.22[44]
E	37.12	56.41	45.65	29.28
	42.88[41]	36.85[70]	31.60[45]	[10.78][44]
CP	3.73	12.98	7.35	14.33
			15.5[48]	14.33
B/G	3.77	4.52	4.10	6.21
	4.81[45]	[1.76][70]	3.44[45]	1.98[44]
ν	0.37	0.39	0.38	0.42
	0.42[41]	0.36[70]	0.37[45]	[0.28][44]
ζ	0.50	0.40	0.37	0.57
	[0.57][41]	0.51[43]	0.37	0.57
λ	41.82	77.91	54.43	57.01
μ	13.46	20.18	16.49	10.28

than that of $AgCoF_3$ (42.88), which signifies that $AgCoF_3$ has greater stiffness or resistance to deformation under an applied force than $AgNiF_3$ but less than $AgCoF_3$. In addition, $AgCrCl_3$ (56.41) has the highest resistance to external stress of all of the studied compounds, i.e., $AgCrF_3$, $AgCrBr_3$, and $AgCrI_3$. It is also a more resistant material than $CsCaCl_3$ (36.35 GGA approximations) and $CsCdCl_3$ (36.85). On the other hand, $AgCrBr_3$ (45.65) is the second-highest stiffening compound in this study and also higher than $KGeBr_3$ (17.94), $RbGeBr_3$ (27.71), and $CsGeBr_3$ (31.60). Finally, $AgCrI_3$ (29.28) has much larger resistance to external force than $LiPbI_3$ (10.78). The mechanical stress at some particular point within a continuum is measured by Cauchy pressure CP. The difference between two elastic constants (C_{12}−C_{44}) is referred to as Cauchy pressure. It can be represented mathematically as follows

$$CP = C_{12} - C_{44} \tag{9}$$

The sign (positive or negative) of the Cauchy pressure can be utilized to predict the type of bonding in a solid. The Cauchy pressure is positive for compounds with dominant ionic bonds and negative for those with dominant covalent bonds.[64] Cauchy pressure, which demonstrates the angular nature of atomic bonding in metals, is related to the ductility of materials.[65] A positive Cauchy pressure often observes a crystal's ductility, whereas brittleness can be identified by a negative value.[66] The calculated Cauchy pressures of $AgCrX_3$(X: F, Cl, Br, and I) are 3.73, 12.98, 7.35, and 14.33, respectively. Cauchy pressure is positive for all the above-mentioned compounds, which means that all the studied compounds ($AgCrF_3$, $AgCrCl_3$, $AgCrBr_3$, and $AgCrI_3$) are ionic and ductile. The Pugh's ratio B/G, also known as the Pugh's modulus ratio, is a relationship between the bulk modulus (B) and the shear modulus (G) of a material. It has been characterized as follows

$$\text{Pugh's} - \text{ratio} = B/G \tag{10}$$

It is a significant factor that categorizes solid materials into ductile and brittle groups, with a critical value of 1.75.[67,68] A material is characterized as brittle when the $B/G < 1.75$, while it is considered ductile when the $B/G > 1.75$, ratio of B to G is more than 1.75.[64] It is clear from the analysis that the compounds $AgCrF_3$, $AgCrCl_3$, $AgCrBr_3$, and $AgCrI_3$ are ductile because they have values of $\frac{B}{G}$ that are greater than 1.75. If we compare the studied materials with the literature (Table 4), it can be seen that all of the materials $KGeF_3$, $RbGeF_3$, and $CsGeF_3$ are also ductile. Similarly, $AgCrCl_3$ is the second-highest ductile material studied in this work and is even more ductile than $CsCaCl_3$. The compound $AgCrBr_3$ has values of ductility much higher than those of $KGeBr_3$ (3.44), $RbGeBr_3$ (2.10), and $CsGeBr_3$ (1.78). Finally, $AgCrI_3$ (6.21) is the most ductile material; it is also more ductile than $LiPbI_3$. The ratio of a material's lateral to longitudinal strain under mechanical force can be defined by the basic mechanical characteristic known as Poisson's ratio (ν). Its mathematical form is

$$\nu = \frac{3B - 2G}{2(3B + G)} \tag{11}$$

In this scenario, bulk modulus B and shear modulus G are both taken into consideration. The Poisson's ratio is a critical parameter that characterizes the mechanical behavior of materials, specifically in terms of their brittleness or ductility. Materials exhibiting a Poisson's ratio below 0.26 are classified as brittle, whereas those with a Poisson's ratio about equal to or over 0.26 are categorized as ductile.[69] Here, the compounds $AgCrF_3$, $AgCrCl_3$, $AgCrBr_3$, and $AgCrI_3$ have a Poisson's ratio that is positive and higher than 0.26 as mentioned in Table 5,

Table 5. GGA + SOC Calculated Total Magnetic Moment (m) of $AgCrX_3$ (X: F, Cl, Br, I) Compounds in Unit of μ_B under Various Strains ϵ

sample	$m(-3\%)$	$m(-2\%)$	$m(0\%)$	$m(+2\%)$	$m(+3\%)$
$AgCrF_3$	3.66	3.67	3.70	3.74	3.75
$AgCrCl_3$	3.87	3.89	3.91	3.93	3.94
$AgCrBr_3$	3.88	3.90	3.92	3.95	3.95
$AgCrI_3$	3.85	3.87	3.91	3.93	3.94

which indicates that they are all ductile in nature. The observed outcome indicates that the compounds under investigation exhibit a propensity to undergo expansion (contraction) in two orthogonal dimensions when subjected to compression (tension) in an alternate direction. This fact is known as the Poisson effect.

The Kleinman parameter (ζ) is another dimensionless parameter that can range from 0 to 1. It is used for fixing cation and anion sublattices for their locations. According to Kleinman's definition, the minimized bond bending component is linked to the lower threshold, while the minimal bond stretching component is related to the higher threshold.[71] The Kleinman parameter (ζ) is defined in terms of elastic constants C_{11} and C_{12}[72]

$$\zeta = \frac{C_{11} + 8C_{12}}{7C_{11} + 2C_{12}} \tag{12}$$

https://doi.org/10.1021/acsomega.3c10174
ACS Omega 2024, 9, 18148−18159

It can be seen from the equation that ζ gains its highest value, if $C_{11} = C_{12}$ as $\zeta = 1$. The parameter proposed by Kleinman has a well-established correlation, wherein a decline in its value corresponds to a boost in resistance to bond bending or bond angle distortion.[73] Presently, the compounds $AgCrI_3$ and $AgCrBr_3$ have the highest and lowest values of ζ, which indicates that they have the smallest and largest oppositions to bond bending or bond angle distortion. $AgCrF_3$ and $AgCrCl_3$ also have lower bond bending bond angle distorting compared to $AgCrBr_3$. Lamé parameters are a pair of material-specific quantities denoted as μ and λ, which are used in the formulation of strain−stress relationships. These quantities are sometimes referred to as the Lamé coefficients, Lamé constants, or Lamé moduli.[74] Typically, Lamés first parameter and Lamé's second parameter are denoted by μ and λ, respectively. In the realm of elasticity, the shear modulus, denoted as μ, is the designated nomenclature, and G may serve as a substitute for μ. The use of Young's modulus E is often linked with the symbol G, whereas the parameter μ is frequently matched with the symbol λ.[75] The μ and λ are defined as

$$\mu = \frac{E}{2(1+\nu)} \tag{13}$$

$$\lambda = \left(\frac{\nu E}{(1+\nu)(1-2\nu)}\right) \tag{14}$$

Using GGA + SOC calculations, Lame's parameters have been calculated. which shows that Lamé's second modulus is approximately Voigt's shear modulus. On the other hand, there is a connection between a portion of Young's modulus and the first Lamé modulus. This is something that can be easily shown: $\lambda = C_{12}$ and, $\mu = \frac{(C_{11}-C_{12})}{2} = C_{44}$ for an isotropic system.However, $AgCrX_3$ (X: F, Cl, Br, I) are substantially anisotropic materials, so our calculated results do not satisfy the above relations, which only apply to isotropic systems.

3.3. Phonon B and Structure. The finite displacement method was used to calculate the second-order interatomic force constants (IFCs-2) harmonic terms using PHONOPY code.[76] The IFCs-2 were computed using a 4 × 4 × 1 supercell containing 48 atoms, and the total energies were obtained using point meshes of 5 × 5 × 1. The graph in Figure 2a−d displays the phonon band structure along the high symmetry points that form a closed path Γ−M−K−Γ in the first Brillouin zone. Notably, a negative frequency exists at the M point in the phonon band structure due to the slight variations in the lattice constant. Besides this, it is small in magnitude and can be neglected. All of the phonon band structures show positive frequency at the Γ point, indicating the compounds being studied are kinetically stable.

3.4. Electronic Structure. The electronic properties of a material include the conductive behavior of electrons, their distribution across energy levels, arrangement of electronic structures, and response to the external field. The qualities above are paramount in influencing the conductivity and magnetic properties of the components. Figure 2a−e shows the band structure, and 3a−d represents total density of states (TDOS) and partial density of states (PDOS) of the $AgCrF_3$ compound.

The electronic band structure, TDOS, and PDOS of the mentioned compounds $AgCrX_3$ (X: F, Cl, Br, and I) show similar behavior [see Figures S1a−dS3a−d], which is why we present only here data for one compound $AgCrF_3$, and the remaining data is moved to Supporting Information. To compute the band structures at the high symmetry points Γ − X − M − Γ − R − M, a range of energy from −6 to 6 eV is used. The Fermi level is shifted to 0 eV. The spin-up and spin-down channels cross the Fermi level, as shown in the spin-polarized band structure (see Figure 2a−e). Employing the GGA + SOC calculations confirms the metallic and magnetic nature of the studied halide perovskite $AgCrX_3$ (F, Cl, Br, I) compounds, which exhibit metallic and magnetic behavior even when no strain is applied (ϵ = 0%) [see Figure 2c]. The energy bands that are only half-filled cross the Fermi level, giving the bands metallic character. The investigation also involves the analysis of the TDOS and partial densities of state (PDOS) of $AgCrX_3$ (F, Cl, Br, I) at zero strain, as shown in Figure 3a−d. This approach aims to provide a comprehensive

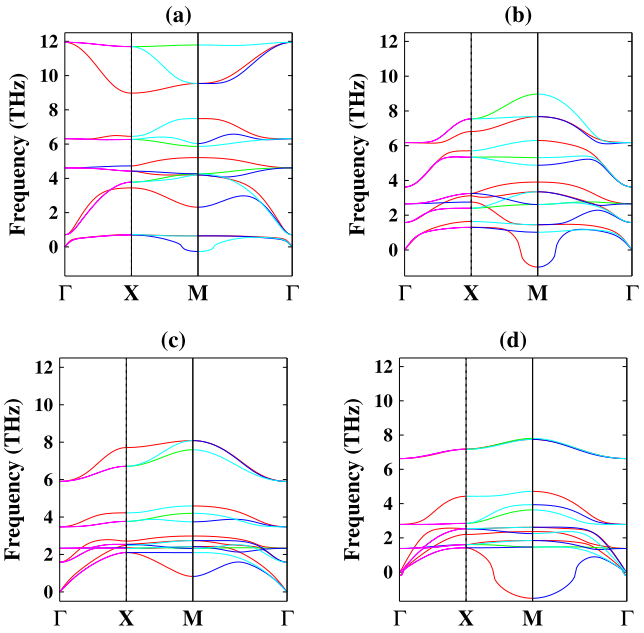

Figure 2. Phonon band structure of (a) $AgCrF_3$, (b) $AgCrCl_3$, (c) $AgCrBr_3$, and (d) $AgCrI_3$ at equilibrium lattice constant.

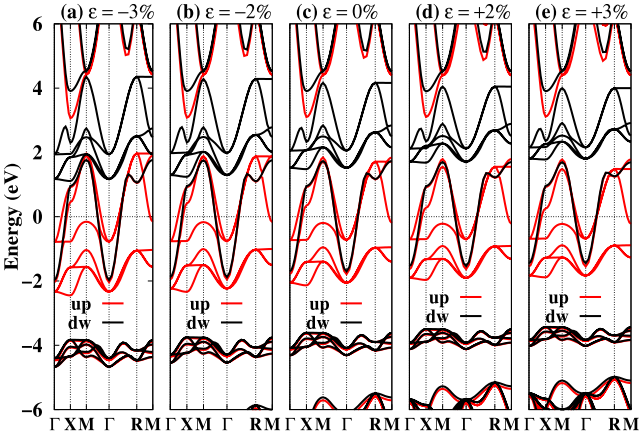

Figure 3. Spin-polarized band structure of a halide perovskite $AgCrF_3$ crystal structure under 0 to ±3% volumetric strain: (a) ϵ = −3%, (b) ϵ = −2%, (c) ϵ = 0%, (d) ϵ = +2%, and (e) ϵ = +3%. The spin-up and spin-down channels are represented by dotted red and solid black lines, respectively.

https://doi.org/10.1021/acsomega.3c10174
ACS Omega 2024, 9, 18148−18159

understanding of those compounds' electronic characteristics. The investigation indicates that the spin-up and spin-down channels cross the Fermi level, confirming the materials' metallic nature at the equilibrium lattice constant. The nonperfectly symmetrical TDOS and PDOS have demonstrated magnetic behavior in these compounds.

Figure 3a–d shows that at zero strain (ϵ = 0%), the valence band in $AgCrF_3$ is dominated by the d-orbital of Cr atom with minor contribution from Ag p-orbital and F atom s-orbital states. While moving from $AgCrF_3$ to $AgCrI_3$, the contribution of the d-orbital of Cr atom keeps on increasing along with the contribution of p-orbitals of Ag and halogen atoms [see Supporting Information Figure 3a–d]. Except for the case of $AgCrCl_3$ in which the valence band is due to the major and minor contribution of d-orbitals of the Cr atom and Ag atom, respectively [see Figures S4a–d–S6a–d]. On the other, the conduction bands are formed due to the prominent contribution of orbitals of Ag atoms along the d-orbitals of Cr atoms in all compounds, i.e., $AgCrX_3$ (F, Cl, Br, I). It is also clear from the PDOS that near the Fermi level in the conduction band, the p-state of Ag atom hybridized with the p-state of the F atom. The same trend is followed by the atoms in $AgCrCl_3$ compounds, while for the $AgCrBr_3$ ($AgCrI_3$), in CBM, the p-state of Ag atom hybridized with the p-state of Br (I) atom, as well as d-state of Ag atom, of both compounds [see Figures S4a–d–S6a–d]. Furthermore, it is confirmed that the material is ferromagnetic, because the TDOS and PDOS are not symmetric.

These outcomes result at no strain of the halide perovskites $AgCrX_3$ (F, Cl, Br, I), revealing a metallic behavior, which supports the findings established by the band structure above. A further indicator of these compounds' magnetic behavior is the nonsymmetric TDOS and PDOS [see Figures S4–S6]. Figure 2a–e depicts the electronic structure estimated vs strain under different strain. In particular, in light of earlier research that showed that the application of strain could alter the electronic structure materials, their magnetic properties would also be changed. A volumetric strain is used to modify the electronic structure of $AgCrX_3$ (X: F, Cl, Br, I) and to estimate whether it changes its electronic characteristics. Our investigation has found that the Fermi level is slightly changed under the applied strain. Yet, in the strain ranges of ϵ = −3 to +3% except $\epsilon = \pm$ 1%, there's no detectable or significant variation in metallic character for both spin-up and spin-down channels of these compounds $AgCrX_3$ (X: F, Cl, Br, I). Figure 2a–e indicates that under applied volumetric strains, the electronic structure of these compounds does not alter significantly but causes noticeable changes in the magnetic moment that do affect their magnetic properties in a distinguishable way [see Figure 4].

The origin of magnetism, the presence of unpaired electrons, the strength of magnetic interactions between atoms or ions, and so forth are discussed The presence of unpaired electrons in the atom and the asymmetric TDOS, or irregular spin distribution, gives rise to a nonzero magnetic moment in the compounds. The cations Ag^+, Cr^{2+}, and the anion X^- in the $AgCrX_3$ (X: F, Cl, Br, and I) compounds provide electrical neutrality. As the Ag^+ and X^- do not or do participate in magnetism in a minor way, the exchange coupling between Cr^{2+} cations serves as the fundamental governing force of the magnetic behavior. The 3d states of Cr-atoms contribute the dominant contribution in the total and local atomic magnetic moment [see Table 1], which indicates that the other

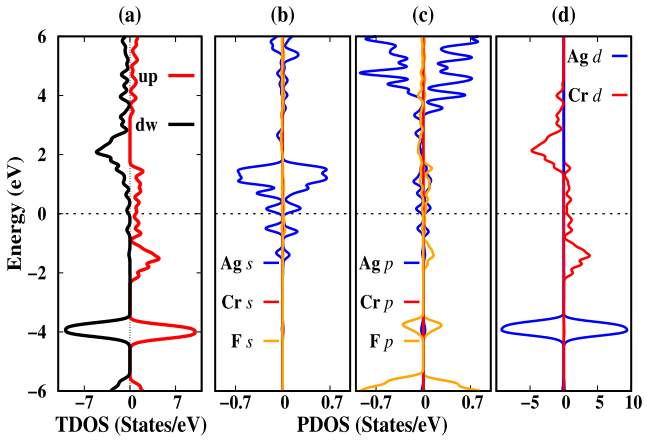

Figure 4. Spin-polarized (a) TDOS and (b) PDOS of s-orbital, (c) PDOS of p-orbital, and PDOS of d-orbital for atoms in $AgCrF_3$ crystal structure at equilibrium lattice constant.

nonmagnetic atoms contribute only a small fraction of magnetic moment. Our calculations of the total magnetic moment of $AgCrF_3$, $AgCrCl_3$, $AgCrBr_3$ and $AgCrI_3$ compounds at different volumetric strains are listed in Table 5.

Hund's Rule states that electrons must occupy every orbit singly before the orbit is doubly occupied. This leaves the atom with unpaired electrons that exhibit a magnetic moment, which results in total magnetization due to their ability to orient in either direction. For example, H has one valence electron, so the isolated H atom is magnetic with a magnetic moment of 1 μ_B, and nitrogen has three valence electrons, so it has a magnetic moment of 3 μ_B.[77] Similarly, isolated Cr^{2+} ion has four valence electrons; we are expected 4 μ_B magnetic moment in Cr-based perovskite compounds. Based in Table 1, it can be observed that $AgCrI_3$ exhibits a higher total magnetic moment compared to $AgCrF_3$, owing to a reduction in the electronegativity (EN) of the halogen atom present in the compound. This decrease in EN values results in the localization of charges around the magnetic atom, thereby escalating the magnitude of magnetic moments. Figure 5 shows that when ferromagnetic

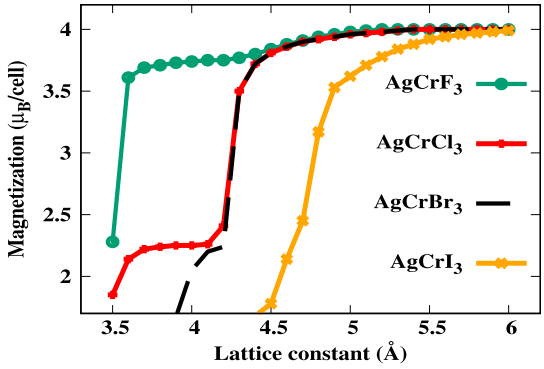

Figure 5. Schematic representations of lattice constant vs magnetization plots of $AgCrX_3$ halide perovskite compounds.

materials are subjected to tensile strain, elongating the bond lengths of magnetic atoms with the surrounding halogen atoms leading to further charge localization on the magnetic atom and increased magnetic moments consistent with the Hund's rule [see Table 5]. Figure 5 provides a visual representation of this phenomenon. In the case of $AgCrX_3$ (X: F, Cl, Br, I), the

https://doi.org/10.1021/acsomega.3c10174
ACS Omega 2024, 9, 18148−18159

local magnetic moment increases under tensile strain, with the magnitude of the strain determining the extent of the increase. According to Table 1, the total magnetic moment of $AgCrI_3$ is greater than that of $AgCrF_3$ due to a decrease in electronegativity (EN) within the same group of elements in the periodic table. The reduction in EN values leads to small charges being transferred from the magnetic atom to the halogen atom; as a result, the calculated total and local magnetic moment increases. Table 5 indicates that when a ferromagnetic material is subjected to tensile (compressive) strain, it can cause the bond lengths of magnetic atoms with halogen atoms to elongate (reduce), further increasing (decreasing) the charge localization around the magnetic atom. In the case of a series of new halides, $AgCrX_3$ (X: F, Cl, Br, I) compounds, the tensile strain has increased the total magnetic moment, depending on the magnitude of the strain.

Figure 4 shows the behavior of magnetization concerning the lattice constants. It can be seen that with the increase of lattice constant, magnetization increases and gains constant values after the optimized lattice constants. This kind of behavior can be observed for all compounds under consideration. For $AgCrF_3$, the magnetization abruptly increases from 2.28 μ_B (at 3.50 Å) to 3.61 μ_B (at 3.60 Å) and gained constant values 4.00 μ_B (at 5.20 Å). While in the case of $AgCrCl_3$, the magnetization increases from 2.41 μ_B (at 4.20 Å) to 3.50 μ_B (at 4.30 Å) and grabs a constant value of 4.00 μ_B (at 5.40 Å). The magnetization of $AgCrBr_3$ compound shows strange behavior as it swiftly increases 0.51 to 1.37 μ_B (from 3.70−3.80 Å) and again 2.05 μ_B (at 4.00 Å) and 3.50 μ_B (at 4.30 Å) and finally gets constant values of 4.00 μ_B (at 5.40 Å). On the other hand, $AgCrI_3$ gets magnetization of 0.24 μ_B (at 4.10 Å) and keeps on increasing from 1.25 μ_B to 2.45 μ_B in the range of lattice constant 4.30−4.70 Å and abruptly increases and gained magnetization of 3.71 μ_B (at 4.80 Å) and finally gets a constant value of 4.00 μ_B (at 6.00 Å).

3.5. Ferromagnetic and anti-Ferromagnetic Interactions. The ferromagnetic ground state in $AgCrX_3$ (X: F, Cl, Br, I) can be roughly confirmed by the total energy difference between E_M (magnetic) and E_{NM} (nonmagnetic). To verify the ground state, we further used FM and AFM interactions to examine the ground state of the compounds. For this, we evaluated ΔE_{FM-AFM} which is defined as

$$\Delta E_{FM-AFM} = E_{FM} - E_{AFM} \tag{15}$$

To confirm whether the halide perovskite compound, $AgCrX_3$ (with X = F, Cl, Br, I), has room-temperature ferromagnetism, we analyzed the interactions between the first, second, and third nearest neighbor spin−spin interactions. The difference in the total energy of various states indicates that spin orientation is crucial. Therefore, the second and third nearest neighbor exchange interactions play a significant role in calculating the Curie temperature for these newly predicted halide perovskite compounds. In our study, we evaluated three possible spin orientations, namely, ferromagnetic (FM), antiferromagnetic 1 (AFM1), and antiferromagnetic 2 (AFM2) configurations [see Figure 6a−c].

In the context of a cubic system, including magnetic centers of equal magnitude, each magnetic center is characterized by the presence of a single unpaired electron residing in a confined atomic orbital. Furthermore, it is worth noting that the interactions between the localized spins are mostly influenced by the closest neighboring magnetic ions. The structural unit cell of such a periodic system has just one

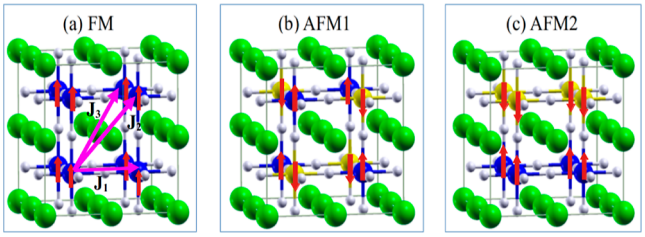

Figure 6. Ball-and-stick model of $AgCrX_3$ for FM and AFM coupling (a) FM state, (b) AFM1 state, and (c) AFM2 state. The blue and yellow colors represent Cr atoms with up and down spin, respectively.

magnetic atom for each material. Therefore, supercells are required in order to achieve the required solutions and make use of the mapping technique, as shown in Figure 4. However, it is anticipated and empirically observed in numerous magnetic systems that two-body interactions will be the primary factor, with nearest-neighbor two-body interactions displaying greater magnitudes. The Hamiltonian equation, commonly known as the Heisenberg (or Heisenberg−Dirac-Van Vleck) Hamiltonian, is often used to describe the simplest scenario involving isotropic two-body interaction magnetic centers.

$$\hat{H} = -\sum_{i,j} J_{i,j}\hat{S}_i\hat{S}_j = -J\sum_{\langle i,j\rangle}\hat{S}_i\hat{S}_j \tag{16}$$

where $\langle i,j\rangle$ indicates that the summation covers all equivalent pairs of nearest neighbor sites only, which is an infinite number in a bulk solid, and J is the two-body spin amplitude, also known as the magnetic coupling constant, between i and j equivalent sites with $\hat{S}_i$ and $\hat{S}_j$ total effective spin operators. The utilization of a minus sign in this context adheres to a tradition that signifies negative J values as indicative of an antiferromagnetic interaction. This interaction implies that a state characterized by antiparallel spins between sites i and j is more stable. The amplitudes of the relevant spin operators are often determined by experimental methods but frequently in an indirect manner due to the necessity of making assumptions regarding the magnitude and polarity of the dominant terms. Ferromagnetic and antiferromagnetic energy can be described by the equation as, $E(FM) = -3J_zS^2$, $E(AFM1) = -JS_z^2$ and $E(AFM2) = +3JS_z^2$. While in our case, S_z is 2. Thus, the ferromagnetic and antiferromagnetic energy difference can be expressed as

$$E_{FM} - E_{AFM1} = 2JS_z^2 \tag{17}$$

$$E_{FM} - E_{AFM2} = 6JS_z^2 \tag{18}$$

In this instance, the value of S_z is equal to 2, and as a result, eqs 18 and 19 will have the following form

$$E_{FM} - E_{AFM1} = 8J \tag{19}$$

$$E_{FM} - E_{AFM2} = 24J \tag{20}$$

To gain insights into the spintronic properties of $AgCrX_3$ (X: F, Cl, Br, I), we calculated the spin density iso-surfaces. Spin density (ρ) is defined as the difference between the electronic densities of spin-up states ($\rho^{\uparrow}$) and spin-down states ($\rho^{\downarrow}$). Figure 8a−f showcases the spin densities of isosurfaces both top and side views of FM (ferromagnetic), AFM1 (antiferromagnetic type 1), and AFM2 (antiferromagnetic type 2) states in the case of the $AgCrF_3$ perovskite compound. The

https://doi.org/10.1021/acsomega.3c10174
ACS Omega 2024, 9, 18148−18159

spin densities appear uniformly distributed around the chromium (Cr) atom, with positive and negative spin densities represented by red and blue dice shapes, respectively [see Figure 7a–f]. In the case of $AgCrF_3$ in FM order (Figure 7a,b),

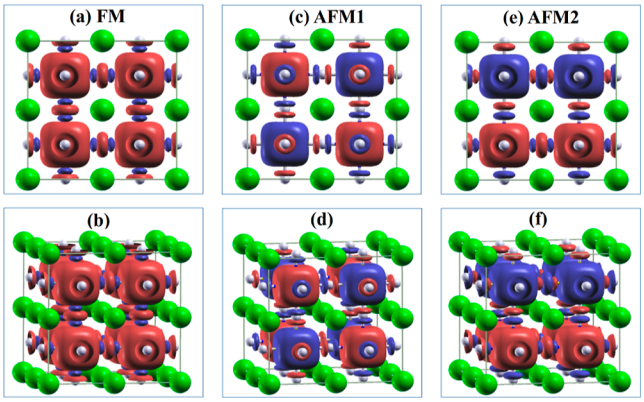

Figure 7. Top and side view of the spin density iso-surfaces of $AgCrF_3$ (a,b) FM state (c,d) AFM1 state, and (e,f) AFM2 state. The value of the iso-surface is 0.001 $eÅ^{-3}$ in all cases. The red and blue colors represent positive and negative spin densities, respectively.

a positive spin density iso-surface is observed in the form of dice shapes (red color) that enclose the Cr atoms prominently in both top and side views. Additionally, a small positive spin density is also observed in the ring shape surrounding the face-centered halogen F atoms. However, Figure 7c,d shows the spin density iso-surfaces of AFM type 1 order in which the positive and negative spin density is alternating. Interestingly, a small ring of positive and negative spin density surrounding the halogen F atom is also observed alternatively. The Cr–F bonds show positive spin density near the negative spin density of Cr atoms, while in contrast, negative spin density near the positive spin density of Cr atoms [see Figure 7c,d]. On the other hand, in the case of AFM2 order, as shown in Figure 7e,f, a uniform positive spin density iso-surface encloses the upper plane of Cr atoms, while negative spin density iso-surface encloses the bottom plane of the Cr atoms. Interestingly, ring-shaped positive spin density taped the negative dice shape spin density in the upper plane of Cr atoms. For the bottom plane, the converse is also true. So, the Cr–F bonds exhibit quite reflective behavior, as they display positive spin density, where the negative spin density is prominent around the Cr atom.

Table 6 shows the ground state energies of FM, AFM1, and AFM2. It is evident from the table that FM is the most stable state. The energy difference between FM and AFM suggests that different spin orientations result in various exchange interactions, highlighting the importance of spin interactions. The exchange coupling constant for the first, second, and third nearest neighbor interactions are given the names J_1, J_2, and J_3, respectively, based on the bond length between them. Table 6 shows J_1 and J_2 values, both of which are negative. This suggests that for all investigated samples, the most stable state is a ferromagnetic state. For these novel halide perovskite $AgCrX_3$ compounds, we compute the Curie temperature using MFT and Monte Carlo simulation, which demonstrates intrinsic ferromagnetism. To perform MFT simulations, we require the first nearest-neighbor exchange interaction. On the other hand, to do realistic calculations of the transition temperature, we considered Monte Carlo (MC) simulations. To perform MC calculations, we need a high-order exchange

Table 6. Total Energies of FM, AFM1, and AFM2 States in Unit of Ry[a]

compounds	$AgCrF_3$	$AgCrCl_3$	$AgCrBr_3$	$AgCrI_3$
E_{FM} (Ry)	−3244.41	−2906.24	−2790.63	−2874.27
E_{AFM1} (Ry)	−3244.37	−2906.20	−2790.60	−2874.25
E_{AFM2} (Ry)	−3244.41	−2906.05	−2790.47	−2874.12
J_1 (meV)	−33.51	−39.53	−33.46	−31.32
J_2 (meV)	−2.45	−2.55	−1.69	−1.38
T^{MFT} (K)	259.16	305.72	258.77	242.22
T^{MC} (K)	518.28	624.30	517.94	497.28

[a]The first, second, and third nearest neighbors exchange interactions J_1, J_2, and J_3 are computed in meV. In all samples, J_3 is calculated 0.0005 meV. Transition temperature *T*cMFT and *T*cMC values are expressed in units of K.

interaction constant. The computed values of J_1, J_2, and J_3 for $AgCrF_3$ halide perovskite sample with a simple cubic crystal structure are −33.51, −2.45, and 0.0005 meV/link, respectively [see Table 6]. Thus, the higher-order term J3 approaches zero, and only the first- and second-nearest-neighbor interactions are significant. So, the different values of the exchange interactions result in different values of transition temperature calculated using MFT and MC calculations.

The fitted data are shown as a red solid line in Figure 8a–d, whereas the data points are shown as a black open circle. The

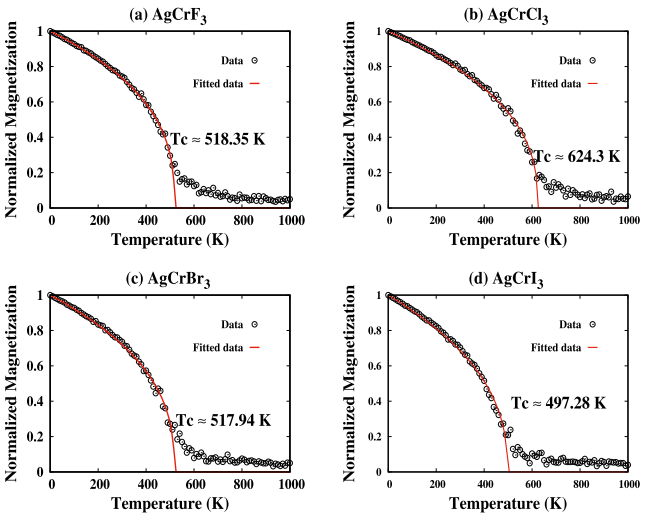

Figure 8. Normalized magnetization is function of temperature calculated using MC simulations: (a) $AgCrF_3$, (b) $AgCrCl_3$, (c) $AgCrBr_3$, and (d) $AgCrI_3$. The empty circle denotes the data point obtained using Monte Carlo simulation, and the solid line indicates the fitted data to the temperature dependent magnetization $M(T) = (1 - T/T_c)^{\beta}$.

normalized magnetizations exhibit a steep decline in the fitted data. This suggests that ferromagnetic to para-magnetic states are undergoing a thermodynamic phase change. For the $AgCrF_3$, $AgCrCl_3$, $AgCrBr_3$, and $AgCrI_3$ compounds, the computed Curie temperatures using MC simulation are 518.35, 624.30, 517.94, and 497.28 K, respectively. The selection of magnetic materials in a wide range of various industrial applications must have unique properties. For example, magnetic materials used in magnetic storage devices, magnetic sensors, magnetic shielding electric motors, and generators depend on their magnetic characteristics, cost, and

https://doi.org/10.1021/acsomega.3c10174
ACS Omega 2024, 9, 18148−18159

stability up to high Curie temperatures. The structural stability, dynamic stability, mechanical stability, and high transition temperature of these compounds indicate the feasibility of synthesis in the experiment. Once it is synthesized, then it is recommended to use these materials in the aforementioned applications.

4. CONCLUSIONS

In this work, we investigated the properties of the new halide perovskite compound $AgCrX_3$ using the DFT method based on GGA + SOC calculations. We investigated the structural, phonon spectrum, elastic, electronic, and magnetic properties of these compounds. Our results indicate that these compounds are structurally and mechanically stable, making them feasible for synthesis in experiments. New $AgCrX_3$ halide perovskite compounds are ferromagnetic above room temperature. Spin-polarized relativistic calculations show conducting behavior in both spin channels, and intrinsic ferromagnetism remains robust under ±3% applied strain. TDOS and PDOS confirm ferromagnetism, and total magnetic moments increase (decrease) under tensile (compressive) volumetric strain. The study found that the *z*-axis is the hard axis of a magnetic atom. The single-ion anisotropy was approximately 0.001 meV in all compounds studied, and using a large supercell of size 3 × 2 × 2 confirmed that it is very small in all cases. We estimated the Curie temperature (T_c) for four different compounds ($AgCrF_3$, $AgCrCl_3$, $AgCrBr_3$, and $AgCrI_3$) using MFT. Our quantum MC simulations provided more accurate estimates of T_c, which were significantly higher for all four compounds. Halide perovskite $AgCrX_3$ compounds could be promising materials for spintronic nanodevices that operate at room temperature.

■ ASSOCIATED CONTENT

Supporting Information

The Supporting Information is available free of charge at https://pubs.acs.org/doi/10.1021/acsomega.3c10174.

Additional details of $AgCrX_3$ halide perovskite compounds under volumetric strain (PDF)

■ AUTHOR INFORMATION

Corresponding Authors

Muhammad Abdul − *School of Integrated Circuit Science and Engineering, University of Electronic Sciences and Technology of China, Chengdu 610054, People's Republic of China*; Email: mabdul@mail.ustc.edu.cn

Altaf Ur Rahman − *Department of Physics, Riphah International University, Lahore 54000, Pakistan*; orcid.org/0000-0001-7772-3272; Email: altaf.urrahman@riphah.edu.pk

Bao Jingfu − *School of Integrated Circuit Science and Engineering, University of Electronic Sciences and Technology of China, Chengdu 610054, People's Republic of China*; Email: baojingfu@uestc.edu.cn

Authors

Muhammad Ahmad − *School of Integrated Circuit Science and Engineering, University of Electronic Sciences and Technology of China, Chengdu 610054, People's Republic of China; Department of Physics, Comsats University Islamabad, Lahore 54000, Pakistan*

Akhtar Rasool − *Department of Physics, University of Sargodha, Sargodha 40100, Panjab*

Misbah Ullah Khan − *Department of Physics, Comsats University Islamabad, Lahore 54000, Pakistan*

Mohammad N. Murshed − *Physics Department Faculty of Science and Arts, King Khalid University, Abha 61421, Saudi Arabia*

Mohamed E. El Sayed − *Physics Department Faculty of Science and Arts, King Khalid University, Abha 61421, Saudi Arabia*

Muhammad Ashfaq Ahmad − *Department of Physics, COMSATS University Islamabad, Lahore 54000, Pakistan*

Complete contact information is available at: https://pubs.acs.org/10.1021/acsomega.3c10174

Notes

The authors declare no competing financial interest.

■ ACKNOWLEDGMENTS

The authors extend their appreciation to the Deanship of Scientific Research at King Khalid University for funding this work through large group Research Project under grant number RGP.2/191/44. We gratefully acknowledge the financial support provided by the research project under grant (A1098531023601318), as well as the National Natural Science Foundation of China grant.

■ REFERENCES

(1) Joshi, V. K. Spintronics: A contemporary review of emerging electronics devices. *Eng. Sci. Technol.* **2016**, *19*, 1503−1513.

(2) Lu, J.; Chen, E.; Kabir, M.; Stan, M.; Wolf, S. Spintronics technology: past, present and future. *Int. Mater. Rev.* **2016**, *61*, 456−472.

(3) Estrada, F.; Guzmán, E. J.; Navarro, O.; Avignon, M. Curie temperature behavior in half-metallic ferromagnetic double perovskites within the electronic correlation picture. *Phys. Rev. B* **2018**, *97*, 195155.

(4) Thompson, S. M. The discovery, development and future of GMR: The Nobel Prize 2007. *J. Phys. D: Appl. Phys.* **2008**, *41*, 093001.

(5) Binasch, G.; Grünberg, P.; Saurenbach, F.; Zinn, W. Enhanced magnetoresistance in layered magnetic structures with antiferromagnetic interlayer exchange. *Phys. Rev. B: Condens. Matter Mater. Phys.* **1989**, *39*, 4828−4830.

(6) Fert, A.; Grünberg, P.; Barthélémy, A.; Petroff, F.; Zinn, W. Layered magnetic structures: interlayer exchange coupling and giant magnetoresistance. *J. Magn. Magn. Mater.* **1995**, *140−144*, 1−8.

(7) De Groot, R.; Mueller, F.; Engen, P. G. v.; Buschow, K. New class of materials: half-metallic ferromagnets. *Phys. Rev. Lett.* **1983**, *50*, 2024−2027.

(8) Lu, Q.; Wang, B.; Chen, X.-R.; Liu, W.-M. Robust large-gap quantum spin Hall insulators in methyl-functionalized III-Bi buckled honeycombs. *Phys. Rev. Mater.* **2018**, *2*, 014005.

(9) Zhang, X.-L.; Liu, L.-F.; Liu, W.-M. Quantum anomalous Hall effect and tunable topological states in 3d transition metals doped silicene. *Sci. Rep.* **2013**, *3*, 2908−8.

(10) Kenmochi, K.; Ann Dinh, V.; Sato, K.; Yanase, A.; Katayama-Yoshida, H. Materials design of transparent and half-metallic ferromagnets of MgO, SrO and BaO without magnetic elements. *J. Phys. Soc. Jpn.* **2004**, *73*, 2952−2954.

(11) An Dinh, V.; Toyoda, M.; Sato, K.; Katayama-Yoshida, H. Exchange interaction and T C in alkaline-earth-metal-oxide-based DMS without magnetic impurities: first principle pseudo-SIC and Monte Carlo calculation. *J. Phys. Soc. Jpn.* **2006**, *75*, 093705.

(12) Spaldin, N. A. Search for ferromagnetism in transition-metal-doped piezoelectric ZnO. *Phys. Rev. B: Condens. Matter Mater. Phys.* **2004**, *69*, 125201.

(13) Rahman, A. U.; Ali, S.; Awan, A. A.; Hayat, S.; Dahshan, A.; Rahman, G. Investigation of room-temperature ferromagnetism in $$ \hbox {SrTiO}_3$$ perovskite structure via substitutional doping. *Eur. Phys. J. Plus* **2021**, *136*, 1137.
(14) Shein, I. R.; Ryzhkov, M.; Gorbunova, M.; Makurin, Y. N.; Ivanovskiĭ, A. L. *Magnetization of Beryllium Oxide in the Presence of Nonmagnetic Impurities: Boron, Carbon, and Nitrogen*; Springer, 2007.
(15) Dinh, V. A.; Sato, K.; Katayama-Yoshida, H. Dilute magnetic semiconductors based on wide bandgap SiO2 with and without transition metal elements. *Solid State Commun.* **2005**, *136*, 1−5.
(16) Rahman, A. U. Strain Induces Ferromagnetism in a Janus Transition Metal Dichalcogenides: CrSTe-1H Monolayer. *J. Electron. Mater.* **2023**, *52*, 1036−1049.
(17) Ur Rahman, A.; Ullah, H.; Verma, M.; Khan, S. Functionalization of monolayer-CdS by metal and non-metal elemental substitution: first-principle understanding. *J. Magn. Magn. Mater.* **2020**, *515*, 167212.
(18) Zhao, X.-G.; Dalpian, G. M.; Wang, Z.; Zunger, A. Polymorphous nature of cubic halide perovskites. *Phys. Rev. B* **2020**, *101*, 155137.
(19) Oleaga, A.; Salazar, A.; Skrzypek, D. Critical behaviour of magnetic transitions in KCoF3 and KNiF3 perovskites. *J. Alloys Compd.* **2015**, *629*, 178−183.
(20) Pena, M.; Fierro, J. Chemical structures and performance of perovskite oxides. *Chem. Rev.* **2001**, *101*, 1981−2018.
(21) Goto, T.; Kimura, T.; Lawes, G.; Ramirez, A.; Tokura, Y. Ferroelectricity and giant magnetocapacitance in perovskite rare-earth manganites. *Phys. Rev. Lett.* **2004**, *92*, 257201.
(22) Bokov, A.; Ye, Z.-G. Recent progress in relaxor ferroelectrics with perovskite structure. *J. Mater. Sci.* **2006**, *41*, 31−52.
(23) Nie, R.; Sumukam, R. R.; Reddy, S. H.; Banavoth, M.; Seok, S. I. Lead-free perovskite solar cells enabled by hetero-valent substitutes. *Energy Environ. Sci.* **2020**, *13*, 2363−2385.
(24) Llanos, M.; Yekani, R.; Demopoulos, G.; Basu, N. Alternatives assessment of perovskite solar cell materials and their methods of fabrication. *Renew. Sustain. Energy Rev.* **2020**, *133*, 110207.
(25) Saiduzzaman, M.; Yanagida, S.; Takei, T.; Kumada, N.; Ogawa, K.; Moriyoshi, C.; Kuroiwa, Y.; Kawaguchi, S. Crystal Structure, Thermal Behavior, and Photocatalytic Activity of $NaBiO_3{\cdot}nH_2O$. *Inorg. Chem.* **2018**, *57*, 8903−8908.
(26) Haq, M. A.; Saiduzzaman, M.; Asif, T. I.; Shuvo, I. K.; Hossain, K. M. Ultra-violet to visible band gap engineering of cubic halide KCaCl 3 perovskite under pressure for optoelectronic applications: Insights from DFT. *RSC Adv.* **2021**, *11*, 36367−36378.
(27) Goel, P.; Sundriyal, S.; Shrivastav, V.; Mishra, S.; Dubal, D. P.; Kim, K.-H.; Deep, A. Perovskite materials as superior and powerful platforms for energy conversion and storage applications. *Nano Energy* **2021**, *80*, 105552.
(28) Bhalla, A.; Guo, R.; Roy, R. The perovskite structure—a review of its role in ceramic science and technology. *Mater. Res. Innovat.* **2000**, *4*, 3−26.
(29) Gómez-Solís, C.; Oliva, J.; Diaz-Torres, L.; Bernal-Alvarado, J.; Reyes-Zamudio, V.; Abidov, A.; Torres-Martinez, L. M. Efficient photocatalytic activity of MSnO3 (M: Ca, Ba, Sr) stannates for photoreduction of 4-nitrophenol and hydrogen production under UV light irradiation. *J. Photochem. Photobiol., A* **2019**, *371*, 365−373.
(30) Khan, R.; Ghafoor, F.; Zhang, Q.; Rahman, A. U.; Waqas Iqbal, M.; Somaily, H.; Dahshan, A. A First-Principles Study of Enhanced Ferromagnetism in a Two-Dimensional Cr-Doped InS Monolayer. *J. Electron. Mater.* **2022**, *51*, 6252−6263.
(31) Hayashi, H.; Inaba, H.; Matsuyama, M.; Lan, N.; Dokiya, M.; Tagawa, H. Structural consideration on the ionic conductivity of perovskite-type oxides. *Solid State Ionics* **1999**, *122*, 1−15.
(32) Lin, W. C.; Tsai, C.; Ogawa, K.; Yamada, S.; Gandhi, A. C.; Lin, J. Interfacial magnetic coupling in hetero-structure of Fe/double-perovskite NdBaMn2O6 single crystal. *Appl. Phys. Lett.* **2018**, *112*, 162403.
(33) Dar, S. A.; Want, B. Predicting and understanding the structural stability, origin of half-metallic magnetic nature, and study of opto-electronic properties of Cs2KXCl6: X= Ti and V double perovskites. *J. Phys. Chem. Solids* **2023**, *174*, 111135.
(34) Giannozzi, P.; Baroni, S.; Bonini, N.; Calandra, M.; Car, R.; Cavazzoni, C.; Ceresoli, D.; Chiarotti, G. L.; Cococcioni, M.; Dabo, I.; et al. QUANTUM ESPRESSO: a modular and open-source software project for quantum simulations of materials. *J. Phys.: Condens. Matter* **2009**, *21*, 395502.
(35) Kohn, W.; Sham, L. J. Self-consistent equations including exchange and correlation effects. *Phys. Rev.* **1965**, *140*, A1133−A1138.
(36) Perdew, J. P.; Burke, K.; Ernzerhof, M. Generalized gradient approximation made simple. *Phys. Rev. Lett.* **1996**, *77*, 3865−3868.
(37) Heyd, J.; Scuseria, G. E.; Ernzerhof, M. Hybrid functionals based on a screened Coulomb potential. *J. Chem. Phys.* **2003**, *118*, 8207−8215.
(38) Monkhorst, H. J.; Pack, J. D. Special points for Brillouin-zone integrations. *Phys. Rev. B: Condens. Matter Mater. Phys.* **1976**, *13*, 5188−5192.
(39) Birch, F. Finite elastic strain of cubic crystals. *Phys. Rev.* **1947**, *71*, 809−824.
(40) Murnaghan, F. D. *The Compressibility of Media under Extreme Pressures*; Proceedings of the National Academy of Sciences, 1944; Vol. *30*, pp 244−247.
(41) Mubarak, A. Ab initio Study of Ag-Based Fluoroperovskite AgMF 3 (M= Co and Ni) Compounds. *J. Electron. Mater.* **2018**, *47*, 887−898.
(42) Murtaza, G.; Murtaza, G.; Khenata, R.; Muhammad, S.; Reshak, A.; Wong, K. M.; Bin Omran, S.; Alahmed, Z. Structural, chemical bonding, electronic and magnetic properties of KMF3 (M= Mn, Fe, Co, Ni) compounds. *Comput. Mater. Sci.* **2014**, *85*, 402−408.
(43) Ghebouli, B.; Ghebouli, M.; Fatmi, M.; Bouhemadou, A. First-principles study of the structural, elastic, electronic, optical and thermodynamic properties of the cubic perovskite CsCdCl3 under high pressure. *Solid State Commun.* **2010**, *150*, 1896−1901.
(44) Awais Rehman, M.; ur Rehman, J.; Bilal Tahir, M. A DFT study of structural, electronic, optical, mechanical, thermoelectric, and magnetic properties of Pb-halide perovskites LiPbX3 (X= Cl, Br, and I) for photovoltaic applications. *Comput. Theor. Chem.* **2023**, *1223*, 114085.
(45) Houari, M.; Bouadjemi, B.; Haid, S.; Matougui, M.; Lantri, T.; Aziz, Z.; Bentata, S.; Bouhafs, B. Semiconductor behavior of halide perovskites AGeX 3 (A= K, Rb and Cs; X= F, Cl and Br): first-principles calculations. *Indian J. Phys.* **2020**, *94*, 455−467.
(46) Körbel, S.; Marques, M. A.; Botti, S. Stability and electronic properties of new inorganic perovskites from high-throughput ab initio calculations. *J. Mater. Chem. C* **2016**, *4*, 3157−3167.
(47) Lamichhane, A.; Ravindra, N. Isosymmetric compression of cubic halide perovskites $$\mathrm{ABX}_{3}$$ ($$A=K, Rb, Cs$$; $$B=Ge, Sn, Pb$$ and $$X=Cl,Br,I$$)-influence of cation−anion exchange: a first principle study. *SN Appl. Sci.* **2021**, *3*, 153.
(48) Shivhare, V.; Khandy, S. A.; Gupta, D. C. Probing the structural, mechanical, phonon, thermal, and transport properties of magnetic halide perovskites XTiBr3 (X= Rb, Cs) through ab-initio results. *Sci. Rep.* **2023**, *13*, 9115.
(49) Rajeswarapalanichamy, R.; Amudhavalli, A.; Padmavathy, R.; Iyakutti, K. Band gap engineering in halide cubic perovskites CsPbBr3- yIy (y= 0, 1, 2, 3)−A DFT study. *Mater. Sci. Eng. B* **2020**, *258*, 114560.
(50) Zandbergen, H.; Ijdo, D. Neutron powder diffraction on RbCrl3 and magnetic measurements on RbCrl3 and CsCrl3. *J. Solid State Chem.* **1981**, *38*, 199−210.
(51) Jamal, M.; Jalali Asadabadi, S.; Ahmad, I.; Rahnamaye Aliabad, H. Elastic constants of cubic crystals. *Comput. Mater. Sci.* **2014**, *95*, 592−599.
(52) Born, M. On the stability of crystal lattices. I. *Math. Proc. Camb. Phil. Soc.* **1940**, *36*, 160−172.
(53) Mouhat, F.; Coudert, F.-X. Necessary and sufficient elastic stability conditions in various crystal systems. *Phys. Rev. B: Condens. Matter Mater. Phys.* **2014**, *90*, 224104.

https://doi.org/10.1021/acsomega.3c10174
ACS Omega 2024, 9, 18148−18159

(54) Baumgart, E. Stiffness-an unknown world of mechanical science. *Injury* **2000**, *31*, B14−B23.
(55) Adams, L. H.; Williamson, E. D.; Johnston, J. The determination of the compressibility of solids at high pressures. *J. Am. Chem. Soc.* **1919**, *41*, 12−42.
(56) Horwood, A., Chockalingam, N., Eds.; *Clinical Biomechanics in Human Locomotion*; Academic Press, 2023; pp 91−174.
(57) Verma, A.; Kumar, A. Bulk modulus of cubic perovskites. *J. Alloys Compd.* **2012**, *541*, 210−214.
(58) Hill, R. The elastic behaviour of a crystalline aggregate. *Proc. Phys. Soc., Sect. A* **1952**, *65*, 349−354.
(59) Irsay, L.; Mandl, P.; Balint, P. V.. In *Essential Applications of Musculoskeletal Ultrasound in Rheumatology*; Wakefield, R. J., D'Agostino, M. A., Eds.; W.B. Saunders: Philadelphia, 2010; pp 29−42.
(60) Zener, C. Interaction between the d-shells in the transition metals. II. Ferromagnetic compounds of manganese with perovskite structure. *Phys. Rev.* **1951**, *82*, 403−405.
(61) Kalpakjian, S. *Manufacturing Processes for Engineering Materials*; Pearson Education India, 1984.
(62) Zhang, H., Ed.; *Building Materials in Civil Engineering*; Woodhead Publishing Series in Civil and Structural Engineering Woodhead Publishing, 2011; p 423.
(63) Yildirim, A.; Koc, H.; Deligoz, E. First-principles study of the structural, elastic, electronic, optical, and vibrational properties of intermetallic Pd2Ga. *Chin. Phys. B* **2012**, *21*, 037101.
(64) Chen, X.-Q.; Niu, H.; Li, D.; Li, Y. Modeling hardness of polycrystalline materials and bulk metallic glasses. *Intermetallics* **2011**, *19*, 1275−1281.
(65) Pettifor, D. Theoretical predictions of structure and related properties of intermetallics. *Mater. Sci. Technol.* **1992**, *8*, 345−349.
(66) Suetin, D.; Shein, I.; Ivanovskii, A. Structural, elastic, electronic and magnetic properties of perovskite-like Co3WC, Rh3WC and Ir3WC from first principles calculations. *Solid State Sci.* **2010**, *12*, 814−817.
(67) Pugh, S. XCII. Relations between the elastic moduli and the plastic properties of polycrystalline pure metals. *London, Edinburgh Dublin Phil. Mag. J. Sci.* **1954**, *45*, 823−843.
(68) Vaitheeswaran, G.; Kanchana, V.; Svane, A.; Delin, A. Elastic properties of MgCNi3—a superconducting perovskite. *J. Phys.: Condens. Matter* **2007**, *19*, 326214.
(69) Frantsevich, I. N. *Elastic Constants and Elastic Moduli of Metals and Insulators*; Reference book, 1982.
(70) Ephraim Babu, K.; Murali, N.; Vijaya Babu, K.; Taddesse Shibeshi, P.; Veeraiah, V. Structural, Elastic, Electronic, and Optical Properties of Cubic Perovskite $CsCaCl_3$Compound: An ab initio Study. *Acta Phys. Pol., A* **2014**, *125*, 1179−1185.
(71) Kleinman, L. Deformation potentials in silicon. I. Uniaxial strain. *Phys. Rev.* **1962**, *128*, 2614−2621.
(72) Harrison, W. A. *Electronic Structure and the Properties of Solids: The Physics of the Chemical Bond*; Courier Corporation, 2012.
(73) Kim, K.; Lambrecht, W. R.; Segall, B. Electronic structure of GaN with strain and phonon distortions. *Phys. Rev. B: Condens. Matter Mater. Phys.* **1994**, *50*, 1502−1505.
(74) Missaghian, P. *Dämpning av seismiska vågor*; KTH, 2018.
(75) Salençon, J. *Handbook of Continuum Mechanics: General Concepts Thermoelasticity*; Springer Science & Business Media, 2012.
(76) Togo, A.; Oba, F.; Tanaka, I. First-principles calculations of the ferroelastic transition between rutile-type and CaCl 2-type SiO 2 at high pressures. *Phys. Rev. B: Condens. Matter Mater. Phys.* **2008**, *78*, 134106.
(77) Ur Rahman, A.; Rahman, G.; Kratzer, P. Enhanced electronic and magnetic properties by functionalization of monolayer GaS via substitutional doping and adsorption. *J. Phys.: Condens. Matter* **2018**, *30*, 195805.

https://doi.org/10.1021/acsomega.3c10174
ACS Omega 2024, 9, 18148−18159